RHEOLOGY AND SOLID FREEFORM FABRICATION: MODELING MATERIAL FLOW IN DEPOSITION TECHNIQUES

R.S. Crockett
Milwaukee School of Engineering, Milwaukee, WI

P.D. Calvert
University of Arizona, Tucson, AZ

Introduction

Deposition is the broad category of Solid Freeform Fabrication techniques that accomplish the layerwise buildup of an object through direct placement of a fluid material in the form of droplets or thin beads. Solidification of a bulk material or binder for ceramic / metal particles is achieved by cooling from a melt (Fused Deposition Modeling[1], Fused Deposition of Ceramics[2], Extrusion Freeform Fabrication[3]) or by polymerization combined with rheology changes which occur as solvent rapidly evaporates during the dispensing process (Extrusion Freeform Fabrication, Reactive Stereodeposition[4]). Post-processing can later be performed on the object as a whole to achieve final properties, such as completion of polymerization or burnout of binder and sintering of ceramic particles.

Objects have been produced from a spectrum of materials, including waxes[1] and thermoplastics such as acrylonitrile-butadiene-styrene (ABS) and medical grade methyl-methacrylate-acrylonitrile-butadiene-styrene (MABS),[5] polyetheretherketone (PEEK), and polymethyl-methacrylate (PMMA).[4] By adding ceramic or metal particles to a thermoplastic binder, silicon nitride,[2] alumina,[4] and stainless steel[6] parts have been produced. Bulk materials and binders that solidify by chemical means have also been successfully demonstrated. Examples include nylon,[7] alumina and silicon carbide particles bound with acrylics,[8] and silica and borosilicate glass objects produced using sol-gel solutions as a binder.[4]

Key to this material flexibility is the ability to operate under a wide range of liquid-to-solid transformation rates; the only requirement in a deposition technique is that a material be dispensed as a fluid and then undergo sufficient solidification to support the next cross-sectional layer. The amount of material flow which occurs during the liquid-to-solid transition is critical, however, as it ultimately impacts the precision and quality of the final object.[9]

The consequences of too rapid a solidification relative to the melt viscosity are increased porosity and poor inter-layer bonding[9] (Figure 1). Additionally, the large contact angles associated with low material flow produces low resolution and noticeable surface roughness. On the other hand, in systems characterized by low viscosity and low solidification rates, avoiding object slump becomes a challenge; this is generally controlled by adjusting the time between placement of adjacent beads (t_1) and layers (t_2) to prevent further shape changes. In certain extremely fluid systems, "balling" of the deposited liquid or "castling" (gaps in the deposited bead) can occur, driven by the surface tension of the liquid.[8] Understanding and controlling the material parameters involved in the initial flow during solidification is thus a requirement for developing new material systems for deposition techniques.

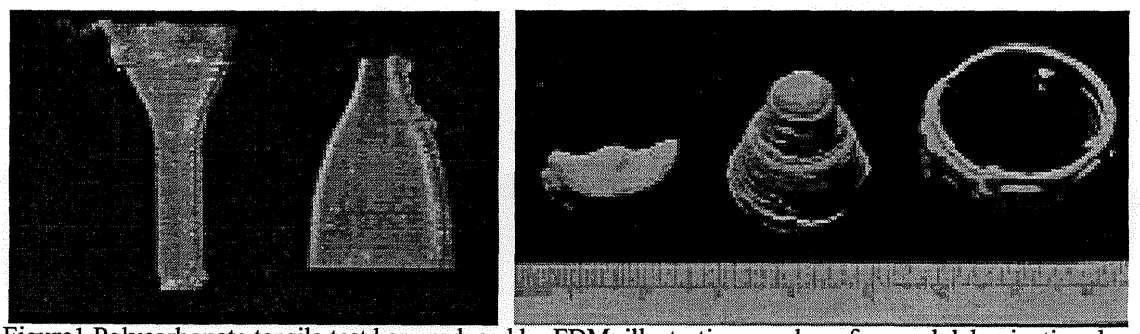

Figure1 Polycarbonate tensile test bar produced by FDM, illustrating rough surface and delamination due to insufficient material flow. Slumping of objects produced by reactive stereodeposition of a silica slurry

Bead Spreading Model

The foundation for a model of a spreading bead of deposited liquid was presented at last year's symposium.[9] The derivation will be published elsewhere.[10] In the model, a bead spreads on the curved surface of the previously deposited layer and is followed as a series of state "snapshots"; surface forces produce an incremental bead deformation in an increment of time. This approach allows flexibility in the time and geometry dependence of the forces associated with a spreading liquid. If the deposited bead conforms to a Bingham-type rheology with a time-dependent yield strength (due to cooling, solvent removal, polymerization) and/or viscosity (due to cooling, changes in the liquid shear rate), it is possible to derive a differential equation for the change in angle over which the bead has spread in an increment of time:

$$\left(\frac{\Delta\phi}{\Delta t}\right)_{x=R\phi} = \frac{1}{32\phi}\frac{\lambda}{\beta}\left[\frac{\cos\phi - \cos(\theta+\phi)}{\phi} - 2\alpha\left(1+\frac{\delta t^{\frac{1}{2}}}{\phi}\right)\right] \tag{1}$$

The above equation is combined with the geometrical relationship between bead spreading angle (ϕ) and bead contact angle (θ) to provide the full solution for bead spreading (see Figure 2):

$$\left(\frac{\sin\theta}{\tan\phi}+\cos\theta\right)^2(\lambda+\phi-\sin\phi\cos\phi) = \theta+\phi-\sin(\theta+\phi)\cos(\theta+\phi) \tag{2}$$

Equation (1) contains a number of parameter groups. In the absence of time-dependent property changes, the final contact angle of a deposited bead is controlled by the dimensionless *strength parameter*, α:

$$\alpha = \frac{\tau_Y R}{\gamma_{LV}} \tag{3}$$

Where τ_y is the yield strength of the liquid, R is the radius of the surface onto which the bead is deposited, and γ_{LV} is the surface tension of the liquid. The rate of bead spreading is controlled by the *time parameter*, β, which has units of (s):

$$\beta = \frac{\eta R}{\gamma_{LV}} \tag{4}$$

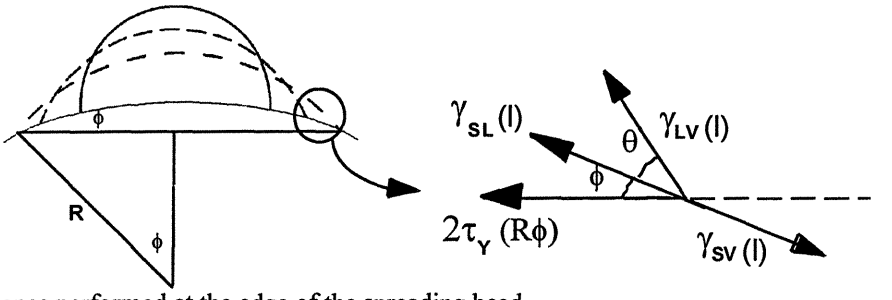

Figure 2 Force balance performed at the edge of the spreading bead.

The time parameter contains the viscosity of the liquid, η. This parameter grouping is the same as that which controls the rate of amorphous material sintering, capillary penetration of liquids, and the dynamic wetting of drops.[11] Note that in deposition techniques, viscosity is rarely a true constant. In the cooling of an amorphous material, it will be a function of bead temperature (thus a function of spreading time). Slurries used in the author's experiments were shear thinning, where viscosity was highly dependent on the shear rate of the liquid (and thus a function of contact angle). The viscosity value in the model is adjusted as required to reflect an average value over the applicable range of temperature or shear rates associated with spreading.

The parameter which controls the diffusion-related property changes of a liquid during solidification is the *strength diffusion coefficient*, δ, which introduces the permeability of the solidifying fluid (P) and the driving force for diffusion (ΔC). δ has units of $s^{-1/2}$:

$$\delta = \frac{(2P\Delta C)^{\frac{1}{2}}}{R}\left(\frac{\tau_{Y,solid}}{\tau_Y} - 1\right) \tag{5}$$

The strength diffusion coefficient represents an increase in the yield strength of the liquid resulting from a surface shell that increases in thickness by diffusion of solvent from the surface or crystallization of a surface layer due to cooling. Finally, bead spreading is dependent on the bead cross-sectional area (A) and substrate radius, represented by the dimensionless *bead geometry parameter*, λ:

$$\lambda = \frac{A}{R^2} \tag{6}$$

Experimental Procedure

To validate the model, dynamic measurements were performed on the spreading of slurries of silica particles in various liquids (ethyl silicate, ethanol, and glycerol). Slurries with a range of α, β, and δ values were prepared by varying slurry surface tension (through liquid selection), viscosity and yield strength (through particle loading and milling time), and amount of volatile ethanol. Two values of λ were obtained by performing all tests on beads with two different cross sectional areas (0.08 mm^2 and 0.32 mm^2). The slurry formulations used in the experiments are presented in Table 1.

Slurry viscosity was determined from the slope of a plot of shear stress measured at various shear rates. Because slurries of silica in ethyl silicate and ethanol are highly shear thinning, single viscosity values were insufficient to describe their behavior over the full spreading process. Average viscosity values were thus determined over the high shear rate range associated with

Table 1 Experimental slurry matrix.

Slurry	Liquid	Loading (vol. %)	Viscosity, initial spreading (N.s/m^2) (shear rate = 3.48 - 17.4 s^{-1})	Viscosity, final spreading (N.s/m^2) (shear rate = 0.09 - 0.17 s^{-1})	Yield (N/m^2)	Surface Energy (N/m)
A	Ethyl Silicate	35	0.24	12.5	2.4	.023
B	Ethyl Silicate	37	0.3	13.5	2.5	.023
C	Ethyl Silicate	39	0.47	13.5	4.7	.023
D	50:50 ETS:EtOH	35.5	0.52	7.0	3.9	.023
E	Ethanol	35	0.15	4.3	5.6	.023
F	Glycerol	0	1.6	1.6	0	.06
G	Glycerol	19	3.18	3.5	0.9	.06

dispensing, 3.5 - 17 s^{-1}, and the low shear rate range typical of continued bead spreading, 0.09 - 0.17 s^{-1}. The data in Table 1 illustrates the nearly two orders of magnitude increase in the values of viscosity for slurries A-E between these shear rate ranges. The glycerol slurries (F&G) were not highly shear thinning, and a single viscosity value was sufficient for the model. Slurry yield strength was calculated from the shear stress vs. shear rate plot as the 0-shear rate extension of a linear curve fit through the lowest measured shear rate.

Slurries were dispensed onto a borosilicate glass rod, with bead width observed as a function of time by a video camera viewing from the underside of the rod. The output of the camera was recorded on S-VHS tape. After the beads were dispensed, the video was reviewed frame-by-frame, with bead width measured by a video measuring system at 0.033 s intervals, as tracked by an onscreen timer (Figure 3).

Results

Full results are available elsewhere;[10] a representative set of experimental results is presented here for illustration. Bead contact angle (θ) as a function of time is plotted as Figure 4 for a bead cross sectional area = 0.08 mm^2. For comparison, time = 0 is taken as when the contact angle reaches 45 degrees. The values of contact angle stop changing at approximately 3 s for ethyl silicate slurries A, B, C. Slurry E (which contained ethanol) reaches a final contact angle much more rapidly, at 0.2 s. The glycerol slurries, F & G, continue to spread and did not reach a final contact angle within the time period of the measurements. The final contact angle increases with

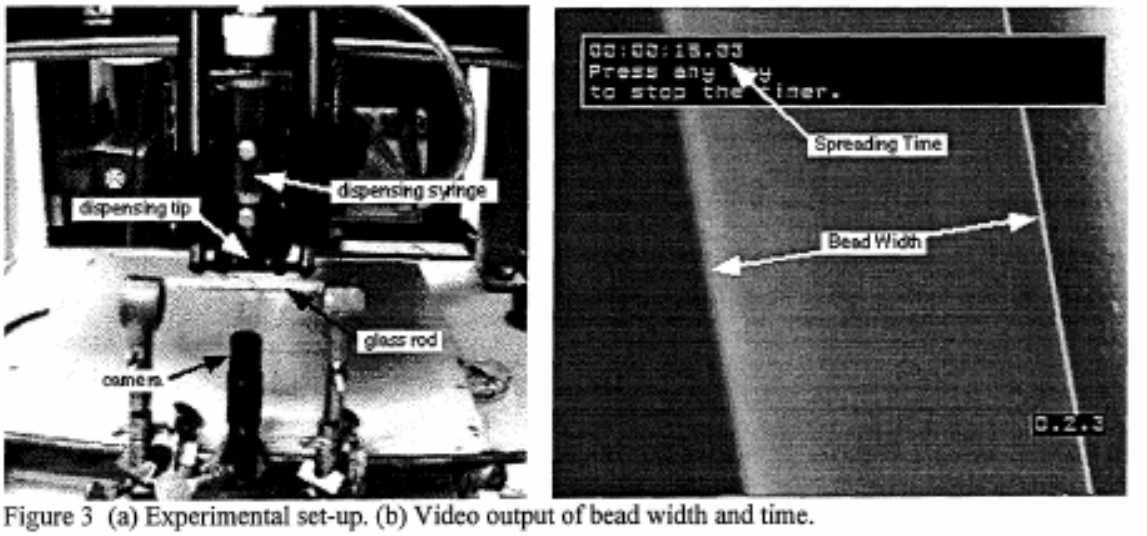

Figure 3 (a) Experimental set-up. (b) Video output of bead width and time.

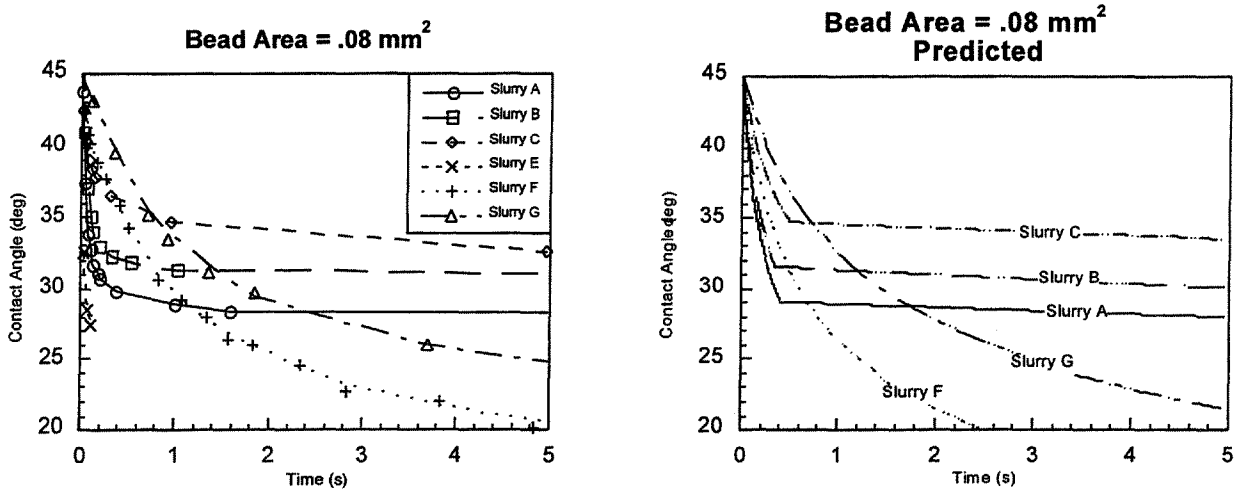

Figure 4 Measured (left) and predicted (right) spreading data.

increasing slurry yield strength, as would be expected. The shape of the curves is dramatically different between the shear-thinning slurries A-E and the non-shear-thinning slurries F & G, although within a given set, the shape of the spreading curve is consistent with decreasing slope with increasing slurry viscosity. Similar curve shape and trends were obtained for bead cross sectional area = 0.32 mm^2, but with higher contact angles and longer spreading times.

Contact angle as a function of time as predicted by the spreading model, using the rheological values of the experimental slurries and A = 0.08 mm^2, is plotted in Figure 4 (right) for the slurries which do not contain solvent. The shear-thinning slurries (A-C) are a composite curve, representing the two viscosity values listed in Table 1. Two predicted values are quantitatively compared in Table 2. These values are: 1) the averaged slope of bead contact angle over time, as represented by the value for the change in contact angle over 5 s, and 2) the final bead contact angle at a small, finite shear rate ($\dot{\varepsilon} = 0.005\ s^{-1}$).

The shape and trends of the model predictions in the early stage of spreading are reasonable when compared to experimental values for slurries which do not involve mass transfer during spreading. Taken over the first 5 s of spreading, the model predicts contact angle changes that vary from experimental results by 6-7%, with a maximum error of less than 17%. The predictions for the final contact angle of shear-thinning slurries, which is expected to be predictable based on a simple equilibrium force balance and independent of slurry viscosity or the selected boundary conditions, are quantitatively poor, however, differing from experimental

Table 2 Change in bead contact angle over 5 s, final contact angle: model predictions vs. actual.

Slurry	Bead Area (mm)	Change in Contact Angle over 5 s (deg, spreading data)	Change in Contact Angle over 5 s (deg, predicted)	% Diff.	Final Angle (deg, calculated)	Final Angle (deg, predicted $\dot{\varepsilon} = 0.005\ s^{-1}$)	% Diff.
A	0.080	16.9	17.0	0.6	28.2	28.8	-2.1
A	0.319	21.0	22.3	6.2	38.2	33.5	12.3
B	0.081	14.0	15.0	7.1	30.6	29.6	3.3
B	0.318	21.0	22.3	6.2	38.9	34.4	11.6
C	0.083	12.5	11.7	-6.4	32.6	34.4	-5.5
C	0.304	13.8	15.6	13.0	46.5	40.9	12.0
F	0.088	25.0	29.0	16.0			
F	0.312	N/A	42.2	N/A			
G	0.081	20.1	23.5	16.9			
G	0.336	32.2	35.0	8.7			

data by as much as 37%. An explanation was developed based on the difficulty of defining a single solidification point for a highly viscous material.[10] An operational definition of solidification as the shear rate beyond which further motion is unlikely, $\dot{\varepsilon} = 0.005\ s^{-1}$, produced predictions for bead final contact angle which were within nominally ± 12% of experimental data. With the model evaluated and shown to provide a reasonable description of the spreading process, the next step is to apply the model to actual deposition systems.

System Contact Angle and Deposition Parameter Space

In an operational deposition system, an object is built up layer-by-layer, not simply by stacking individual beads. Because the outside of a layer is generally deposited first and then the interior filled, however, the surface properties of the object ultimately depend on the single-bead problem developed by the model. After the first few deposited layers, the system will achieve a "system contact angle", where the newly deposited bead spreads until it's final radius equals the radius of the bead onto which it was deposited[9] (Figure 5). Under these equilibrium conditions, the bead geometry parameter, λ, is fixed by the other parameters α, β, and δ. This greatly simplifies analysis by eliminating one system variable and allows the liquid to be plotted on a graphical representation of the α, β, and δ parameter space (Figure 5). The system contact angle in this chart is directly related to the bead contact angle predicted by the spreading model, with large system contact angles producing low part resolution and high surface roughness. System contact angle, θ_{eq}, is determined by the *total* bead strength at equilibrium, which is a function of not only α but also δ, and thus of total spreading time, t:

$$\text{Total Bead Strength} = \alpha\left[1+\delta t^{\frac{1}{2}}\frac{\left(\sin\theta_{eq}+\theta_{eq}\right)^{\frac{1}{2}}}{\frac{\pi}{2}+\frac{\theta_{eq}}{2}}\right] \tag{7}$$

Thus the left axis in Figure 5 contains the parameters α and δ, while the horizontal axis contains β; bead spreading time is read off the chart, and final system contact angle is found on the left axis. This figure may be used in place of a numerical solution to quantify the combined effect of

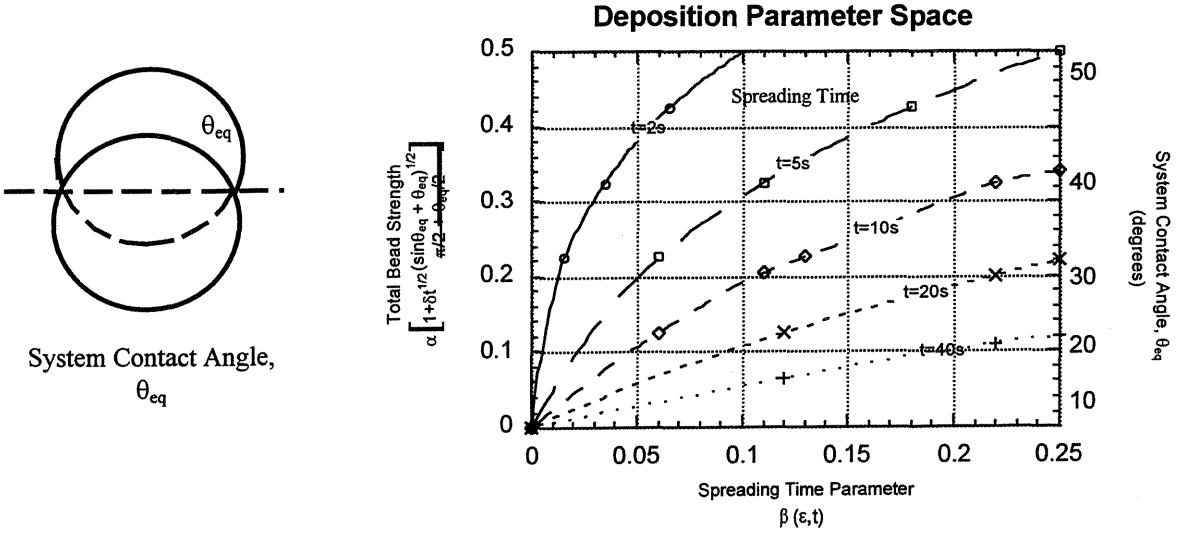

Figure 5 System Contact Angle. Deposition Parameter Space.

all three parameter groupings on bead spreading time and final contact angle. Because of the dependence of system contact angle on spreading time, the spreading time and system contact angle achieved for a given set of α, β, and δ values must be found by iterative use of the chart. Using as an example a deposition liquid with $\alpha = 0.2$, $\beta = 0.1$, and $\delta = 0.1$, the iteration would begin by finding the bead strength / spreading time parameter intersect at $\alpha = 0.2$, $\beta = 0.1$, and $t = 0$ in the total bead strength equation (Equation (7)). These values result a spreading time of approximately 10 s at a system contact angle of 30 degrees. Substituting $\alpha = 0.2$, $\delta = 0.1$, $t = 10$ s, and $\theta_{eq} = 30$ degrees back into Equation (7), the modified value for total bead strength becomes 0.25, corresponding to a spreading time of 7.5 s and a system contact angle of 34 degrees. This process of iteration is repeated until a single value is found for spreading time and system contact angle consistent with the values of α, β, and δ. For the above example, this value is a system contact angle of 31.5 degrees and a spreading time of 8.5 s.

It is also possible to perform a second iteration on this chart for a variable β, to achieve approximate results for cases in which viscosity is not constant throughout the spreading process. For shear thinning slurries, β is a function of shear rate (as represented by θ), and for amorphous thermoplastics, β is a function of t. The iteration would be performed similar to the iteration for bead strength, whereby spreading rate is modified to a new value of β at each new contact angle value or time until a single value is narrowed in on for system contact angle and spreading time.

This chart can be used to provide insight as to how the initial liquid conditions, modified by solidification strategies, will impact the ultimate freeforming characteristics such as object resolution, flaws, and gaps. The bead strength parameter, α, indicates a liquid's resistance to motion. It is in effect a ratio of the restraining force to the driving force for spreading, thus a large α represents a system similar to extrusion, where flow is limited. This is indicated in the schematic of Figure 6 as the region at the top of the chart. Typical systems in this region include the extrusion of engineering thermoplastics; these are characterized by high deposition pressure requirements, high contact angles leading to low object resolution and high roughness, and the possibility for poor interlayer bonding. The time parameter, β, determines the system's spreading rate and response time, with a large β (high viscosity) indicating a slow-moving or "sluggish" system. This is seen in Figure 6 as the region to the extreme right of the chart.

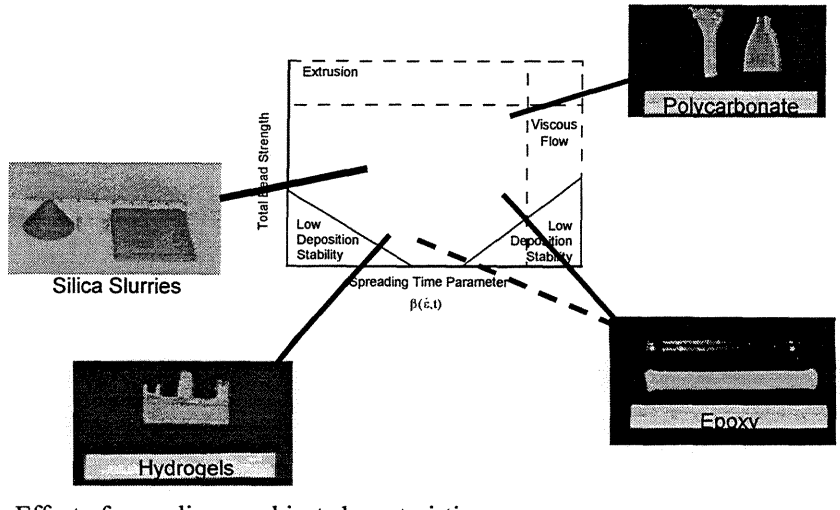

Figure 6 Effect of spreading on object characteristics.

The shaded regions at the bottom of the chart indicate conditions where the liquid may be susceptible to instabilities in the deposition process. One example is the phenomenon of castling, wherein irregularities in deposited lines grow into large peaks and troughs in the course of forming multiple layers. This occurs under conditions of low viscosity and yield strength relative to the liquid surface tension (low $\alpha + \beta$). If the time required for a dispensed bead to reach the surface is greater than some critical value, surface forces will break it into smaller sections. Thus dispensing height becomes an important control parameter to avoid flaws for liquids in this regime. For liquids with low bead strength, α, plus high β, control of dispensing *speed* becomes critical. At large viscosities, a bead will not be able to rapidly "neck down" from a large dispensing orifice; this, combined with low bead strength, will create periodic tears in a deposited bead. This is indicated in Figure 6 by the diagonal shaded region at the bottom right.

An important result from this chart is that proper use of the solidification method can create a workable deposition system from a liquid with "difficult" initial properties. As discussed previously, the time-dependent modifications which can occur during spreading are: 1) viscosity as a function of shear rate (through producing a shear-thinning rheology), 2) viscosity as a function of time (through cooling from a low-viscosity melt), and 3) yield strength as a function of time (through diffusion of mass or thermal energy to the surface). Rheology control, by establishing a shear-thinning slurry such that the viscosity increases during deposition, moves the liquid from its initial placement on the chart horizontally to the right towards longer spreading times. Mass transport, by increasing the yield strength of the fluid in a surface shell, moves it vertically upward in Figure 6 during deposition to higher contact angles. Thermal transport, by modifying the bulk properties of the liquid, generally moves the liquid toward the upper right. Thus initial liquid property characterization and modification, combined with proper selection and control of solidification method, can result in a successful deposition system.

REFERENCES

[1] J.W. Comb, W.R. Priedeman, and P.W. Turley, "FDM Technology Process Improvements," in *1994 Solid Freeform Fabrication Symposium Proceedings*. Austin, TX: University of Texas at Austin (1994) 42-49.

[2] M.K. Agarwala, *et. al.*, "Structural Ceramics by Fused Deposition of Ceramics", in *1995 Solid Freeform Fabrication Symposium Proceedings*. Austin, TX: University of Texas at Austin (1995) 1-8.

[3] P. Calvert R. Crockett, J. Lombardi, J. O'Kelly, and K. Stuffle, "Extrusion Methods for Solid Freeform Fabrication", in *1994 Solid Freeform Fabrication Symposium Proceedings*. Austin, TX: University of Texas at Austin (1994) 50-55.

[4] R.S. Crockett, J. O'Kelly, P.D. Calvert, B.D. Fabes, K. Stuffle, P. Creegan, and R. Hoffman, "Predicting and Controlling Resolution and Surface Finish of Ceramic Objects Produced by Stereodeposition Processes", in *1995 Solid Freeform Fabrication Symposium Proceedings*. Austin, TX: University of Texas at Austin (1995) 17-24.

[5] W. Priedeman, "Thermoplastics for Fused Deposition Modeling (FDM)", in *1996 Solid Freeform Fabrication Symposium Proceedings*. Austin, TX: University of Texas at Austin (1996).

[6] M.K. Agarwala, *et. al.*, "Fused Deposition of Ceramics and Metals: An Overview", Poster presented at *1996 Solid Freeform Fabrication Symposium Proceedings*. Austin, TX: University of Texas at Austin (1996).

[7] J. Lombardi, G. George, L. Rintoul, and P. Calvert, *Polymer Preprints*, **37** [1] (1996) 221-222.

[8] P. Calvert and R. Crockett, "Chemical Solid Free-Form Fabrication: Making Shapes without Molds" *Chem Mater.* **1997** [9] 650-663.

[9] R.S. Crockett and P.D. Calvert, "The Liquid-to-Solid Transition in Stereodeposition Techniques", in *1996 Solid Freeform Fabrication Symposium Proceedings*. Austin, TX: University of Texas at Austin (1996) 257-264.

[10] R.S. Crockett and P.D. Calvert, submitted to Journal of Materials Research, September 1997.

[11] See, for example, J.S. Reed, "Introduction to the Principles of Ceramic Processing," John Wiley and Sons, New York, 1988.